Structure and mechanism in a second-order statistical state dynamics model of self-sustaining turbulence in plane Couette flow

Brian F. Farrell
School of Engineering and Applied Science, Harvard University

Petros J. Ioannou*
Department of Physics, National and Kapodistrian University of Athens

(Dated: July 19, 2016)

This paper describes a study of the self-sustaining process (SSP) that maintains turbulence in wall-bounded shear flow. The study uses Couette flow and is based on a statistical state dynamics (SSD) model closed at second order with state variables the streamwise mean (first cumulant) and the covariance of perturbations (second cumulant). The SSD is closed by either neglecting or stochastically parameterizing the perturbation–perturbation nonlinearity in the perturbation covariance equation. This class of quasi-linear SSD models, which are referred to as RNL models, are a second order SSD systems that includes the stochastic structural stability theory (S3T or equivalently RNL_∞) model which is used in this study. Comparisons of turbulence maintained in DNS and RNL simulations have demonstrated that RNL systems self-sustain turbulence with a mean flow and perturbation structure consistent with DNS. The current results isolate the dynamical components sustaining turbulence in the S3T system concentrating on the parametric instability by which the streamwise mean flow maintains the perturbation field while in turn being maintained by these perturbations. Isolation of this Lyapunov mechanism allows simplification and detailed characterization of the dynamics, structure and energetics of the perturbations maintaining the SSP. In addition, analysis of the interaction between the mean snd perturbation components supporting the Lyapunov instability allows identification and characterization of the mechanism by which the statistical mean state of the turbulence is enforced by the nonlinear feedback control process operating between them.

INTRODUCTION

In this work the mechanism sustaining and regulating turbulence in wall bounded shear flows is studied. Understanding how the turbulent state is sustained against dissipation requires understanding the mechanism by which energy is systematically transferred from the externally driven mean flow to the turbulent fluctuations in the absence of fast inflectional instability of the mean velocity profile. Understanding how the statistical mean state of the turbulence is maintained requires understanding the mechanism by which interaction between the mean and perturbation fields establishes and enforces their observed statistical state. The ubiquitous roll and streak structure, which was first identified in the buffer layer [1], is known to play a key role in sustaining the turbulent state. While this structure is stable in plane wall-bounded flows, it is associated with rapid transient growth producing robust energy transfer from the mean wall-normal shear to the perturbation field when excited by an optimally configured perturbation [2, 3]. This growth results from the streamwise roll circulation giving rise to a streamwise streak through the lift-up mechanism [4]. What is not understood is how this mechanism is maintained in the absence of a linear instability. An early proposed resolution of this conundrum was that these structures participate in a regeneration cycle in which new streaks arise from perturbations the origin of which is ascribed to the break-up of previously formed streaks [5, 6]. This proposed cycle can be viewed as a nonlinear instability mechanism in which turbulence is sustained by energy transfer from the externally forced shear to the perturbation field due to the linear non-normal lift-up growth processes with this non-normal growth being in turn sustained by the continual reformation of the roll and streak structures by the perturbation–parturbation advective nonlinearity. Alternative nonlinear instability mechanisms by which the perturbation advective nonlinearity could sustain the regeneration cycle of rolls and streaks have been the subject of study since this cycle was first posited. Here we refer to these mechanisms collectively as self-sustaining processes (SSP's).

One class of SSP is based on spanwise inflection of the streak velocity profile giving rise to unstable eigenmodes. In this SSP the Reynolds stresses associated with these modes sustain the roll circulation [7–10]. However, subsequent work indicated that streaks are generally too weak to be significantly unstable and an alternative SSP was postulated in which transient growth rather than modal instability maintains the perturbations that force the roll [11]. An advantage of the transient growth SSP is that the postulated optimal perturbations generally exploit the energy of the wall-normal shear in addition to the spanwise shear that primarily supports the inflectional instability. In fact, the mostly rapidly growing perturbations in shear flow in general are oblique waves which optimally exploit the large reservoir of energy in the wall-normal shear [12]. Moreover, the Reynolds

stresses arising in association with the optimal growth of oblique waves associated with streaks have been shown to give rise to the strong systematic forcing of the roll circulations required to maintain the streak [13]. Therefore, it is at least consistent that oblique waves are commonly observed to accompany streaks in wall-turbulence [11].

While the SSP mechanism addresses the question of how the roll and streak structure is destabilized by nonlinear feedback it leaves open the question of how this instability is regulated to zero mean growth and more generally how the turbulence is maintained in the observed statistical equilibrium state. Previously we studied the SSP in a statistical state dynamics (SSD) framework using the Stochastic Structural Stability Theory (S3T) system [14]. In this work we extend that study to examine further both the SSP and its regulation. S3T is an SSD consisting of a second order closure of the dynamics comprising the joint evolution of the streamwise constant mean flow (first cumulant) and the ensemble second order perturbation statistics (second cumulant). The S3T dynamics is closed either by parameterizing the third cumulant using stochastic excitation [15–17] or by setting it to zero, see e.g. [18–20]. Restricting the Navier-Stokes (NS) equations to the first two cumulants in this way retains the nonlinear interaction between the perturbation Reynolds stresses and the mean flow but does not retain the streamwise varying perturbation–perturbation nonlinearity. We regard S3T as an implementation of SSD in the reduced nonlinear (RNL) framework, which is a quasi-linear restriction that neglects the perturbation-perturbation nonlinearity in the dynamics of the second cumulant. The effective number of perturbation ensemble members involved in estimating the second cumulant in the S3T implementation of SSD is infinite so this model is referred to as the RNL_∞ implementation. In RNL more generally the ensemble is approximated by a finite set of perturbations and therefore some fluctuations arising from the stochastic closure remain in the simulation. The RNL_∞ closure is especially amenable to analysis because it results in a nonlinear, autonomous, and deterministic dynamical system governing evolution of the statistical state of the turbulence. In the SSP operating in the RNL_∞ system, it has been shown that transiently growing perturbations tap the energy of the streamwise mean shear to maintain the roll. However, unlike previously proposed transient growth based mechanisms in which the optimal perturbations are presumed to arise adventitiously from break-down of the streak [11, 21], the transiently growing perturbations in S3T turbulence result from systematic parametric instability[22] of the time-dependent streak [13]. Consistently, the structure of the turbulent perturbations is that of the top Lyapunov vector parametrically unstable time-dependent mean flow. This result identifies analytically the structure of the turbulent perturbations. The growth rate of this top Lyapunov vector is verified to vanish, consistent with its constituting the perturbation component of the turbulent state trajectory. Vanishing of the top Lyapunov exponent is brought about by the feedback between the fluctuating mean flow and its associated Lyapunov vector. This result allows identification of the mechanism regulating the turbulent state in the RNL_∞ system but the physical details of this mechanism remains to be elucidated. Nevertheless, knowing the analytical structure of the the perturbations and of the control process regulating the turbulent state allows us to characterize RNL_∞ turbulence to an extent not possible in the full Navier-Stokes system.

In previous work the turbulence supported in RNL systems was shown to closely parallel that in DNS [23, 24]. This similarity between the turbulence observed in RNL simulations and DNS suggests that the RNL and DNS SSPs share an underlying mechanism. Motivated by this similarity we will exploit the relative simplicity of the RNL_∞ SSP to gain insight into the SSP and its regulation in NS turbulence.

This paper is organized as follows. The next section illustrates the similarity of turbulence arising from simulations of the RNL and NS systems. Following that, section formulates the RNL system from its SSD by first reviewing the basics of the theory and then embedding the RNL within the framework of SSD. Section describes the synchronization procedure used in this study then in section the results of numerical experiments using synchronized systems are reported. These simulations were designed to probe in detail the parametric Lyapunov SSP producing and maintaining the perturbations and the feedback process regulating the turbulence to a statistical steady state. This discussion is reported in section .

SIMILARITY OF RNL AND NS TURBULENCE

The turbulence maintained in the RNL system is similar to the turbulence seen in DNS as was demonstrated in recent work in which the structure of the mean flow and of the perturbations in the RNL system and DNS were compared [24–28]. An example snapshot of the roll streak structure in RNL and DNS for the case of $R = 600$ and a channel with $L_z = 1.2\pi$ and $L_x = 1.75\pi$., is shown in Fig. 1. The large-scale roll structures characteristic of turbulent flow are evident in both simulations. The quantitative similarity in these quantities is evident in Fig. 2, which depict comparisons of the temporal spectra of the roll and streak structures in the DNS and RNL simulations. The results in Fig. 1 along with those reported in [24] imply that the RNL system captures fundamental features of fully developed turbulence in plane Couette flow.

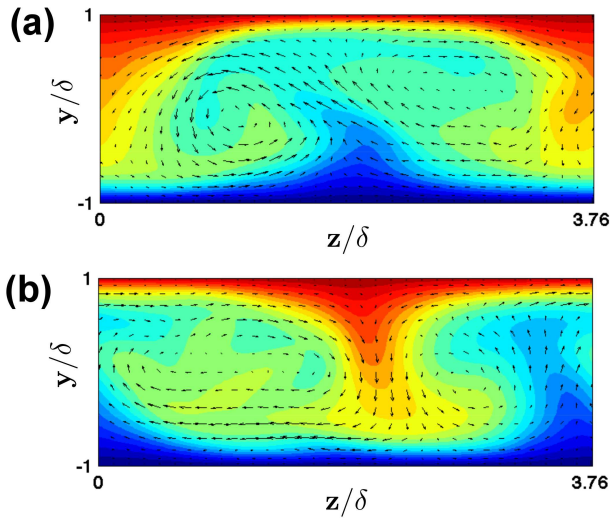

FIG. 1: A y-z plane cross-section of the streamwise constant structure (component $k_x = 0$) of the flow at a single snapshot in time for a (a) DNS and a (b) RNL simulation. Both panels show contours of the streamwise component of the streamwise component of streamwise averaged the mean flow U with the velocity vectors of wall-normal and spanwise components (V,W) superimposed.

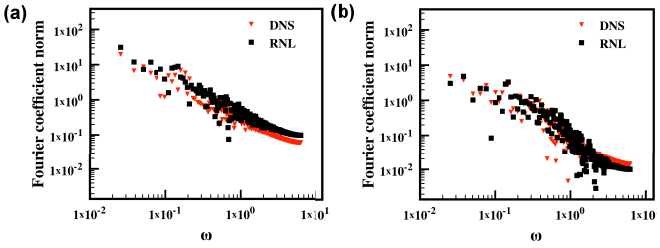

FIG. 2: A comparison of the Fourier spectrum of a DNS (red triangles) and a RNL simulation (black squares) for the (a) streak $\sqrt{(\mathbf{U} - [\mathbf{U}])^2}$ and (b) the roll $\sqrt{V^2 + W^2}$, where (U, V, W) is the streamwise averaged mean flow and $[\,\cdot\,]$ indicates a spanwise average.

THE RNL MODEL AS A STATISTICAL STATE DYNAMICS

Consider an incompressible unit density fluid satisfying the non-dimensional Navier-Stokes equations:

$$\partial_t \mathbf{u} = \mathbf{P_L}\left(-\mathbf{u}\cdot\nabla\mathbf{u} + \frac{1}{R}\Delta\mathbf{u}\right) \ , \qquad (1)$$

where $\mathbf{u}(x, y, z, t) = (u, v, w)$ is the velocity field with streamwise (x) component u, cross-stream (y) component v, and spanwise (z) component w, $\mathbf{P}_L$ is the Leray projection that enforces non-divergence of the flow velocity $\nabla \cdot \mathbf{u} = 0$ [29], and R is the Reynolds number. The flow is confined to a channel with periodic boundary conditions in the streamwise (x) and spanwise (z) directions and no slip boundary conditions at the solid walls $\mathbf{u}(x, y = \pm 1, z) = \pm 1\ \hat{\mathbf{x}}$, which maintain asymptotically and in the absence of turbulence a laminar Couette flow $\mathbf{u} = y\ \hat{\mathbf{x}}$, with $\hat{\mathbf{x}}$ the unit vector in the x direction.

To obtain the statistical state dynamics (SSD) for this turbulent Couette flow we form the equal time cumulants of the state variables and use the method of Hopf to obtain the evolution equations for the cumulants [30–32]. The first order cumulants of the state variables are the means of the variables while the second order cumulants are the spatial covariance of the state variables between two points $\mathbf{x}_1$ and $\mathbf{x}_2$, $\mathbf{C}_{12}$. Translational invariance of the Couette problem in x together with the ergodic assumption, which in this circumstance implies that ensemble means are equal to streamwise means, motivates adopting streamwise means in forming the cumulants. Translational invariance of the problem in x also implies that the second order cumulants are homogeneous functions of the streamwise, (x), direction, i.e. they have the form $\mathbf{C}(x_1 - x_2, y_1, y_2, z_1, z_2, t)$, and as a result $\mathbf{C}_{12}$ has Fourier decomposition of the form:

$$\mathbf{C}_{12} = \sum_{\substack{k=-n \\ k\neq 0}}^{k=n} \mathbf{C}_{k,12} e^{ik(x_1 - x_2)} \ , \qquad (2)$$

In (1) the notation $\mathbf{C}_{k,1,2} \equiv \mathbf{C}(k, y_1, y_2, z_1, z_2, t)$ refers to the covariance of two points in the $y-z$ plane associated with streamwise wavenumber k and n is the total number of streamwise wavenumbers retained in the dynamics.

If the full cumulant expansion is truncated at second order and the third order cumulant is set to zero a closed dynamics for the evolution of the first two cumulants of the flow, which is referred to in other contexts as the second order cumulant expansion (CE2) approximation to the full SSD [18, 32], is obtained. Alternatively, the third order cumulant can be parameterized using a Gaussian random process with second order cumulant components $\mathbf{Q}_{k,1,2}$. Both of these closures have been used previously to study Couette flow turbulence [13]. Despite the severity of the approximation of keeping only two cumulants in the RNL and RNL$_\infty$ systems dynamics, the turbulence in these systems closely parallels Navier-Stokes turbulence [13, 23, 24].

If the second order cumulant field is supported by a single streamwise component wavenumber, k, the RNL$_\infty$ system approximation to the full SSD converges to the

coupled system of equations with matrix form:

$$\partial_t \mathbf{U} = \mathbf{P}_L \left(-\mathbf{U} \cdot \nabla \mathbf{U} + \frac{1}{R} \Delta \mathbf{U} \right) + \mathcal{L}_k \mathbf{C}_k, \qquad (3a)$$

$$\partial_t \mathbf{C}_k = \mathbf{A}_k(\mathbf{U})\, \mathbf{C}_k + \mathbf{C}_k\, (\mathbf{A}_k(\mathbf{U}))^\dagger + \mathbf{Q}_k. \qquad (3b)$$

When $\mathbf{Q}_k \neq 0$, an infinite ensemble of perturbation realizations is retained and the system is fluctuation free and autonomous; we refer to this RNL_∞ equivalent system as S3T. If a single ensemble member is retained the approximation to S3T is imperfect and fluctuations remain; this system will be referred to as RNL_1. The S3T model corresponds to the CE2 approximation if $\mathbf{Q}_k = 0$ in the above equations. The operator $\mathbf{A}_k(\mathbf{U})$ is specified in Appendix A. This operator is linear but is in general time-dependent as it depends on the mean flow $\mathbf{U}$. The equations above are expressed in matrix form which is appropriate for state variables that have been discretized. The continuous operator counterparts have the same form, as discussed in Appendix A.

In this paper we present results only for the case with $R = 600$ in a channel with $L_z = 1.2\pi$ and $L_x = 1.75\pi$ with the eddy field having the single streamwise wavenumber $k = 2\pi/L_x$. For the simulations we have taken 20 discretization points in z and 21 in y. Because the eddy field has a single harmonic the subscript k will be omitted from now on.

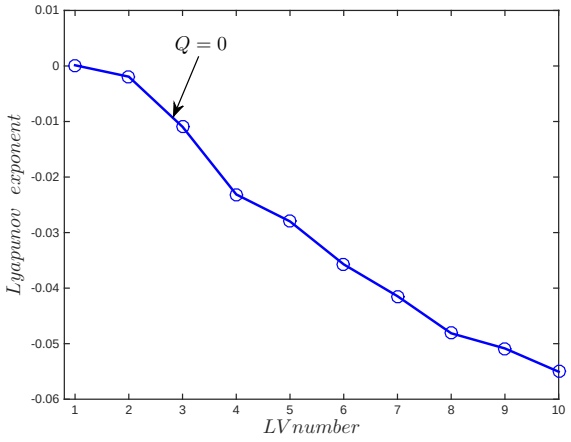

FIG. 3: The first ten Lyapunov exponents of the dynamical operator $\mathbf{A}(\mathbf{U})$ that governs the synchronized system perturbation dynamics. The line connects Lyapunov exponents of the RNL_∞ dynamics without excitation ($\mathbf{Q} = 0$) and, consistently, the maximum Lyapunov exponent (MLE) is zero for this case. Note that because the covariance is a quadratic quantity the corresponding Lyapunov exponents for the covariance are twice the values reported here.

SYNCHRONIZATION OF TWO S3T SYSTEMS

Consider coupling two S3T systems denoted a and b, by setting $\mathbf{U}_b = \mathbf{U}_a$. The first question we address is whether this coupling of only the mean flows results in synchronization of the perturbation fields as well. The dynamics of the coupled S3T systems is governed by:

$$\partial_t \mathbf{U}_a = \mathbf{P}_L \left(-\mathbf{U}_a \cdot \nabla \mathbf{U}_a + \frac{1}{R} \Delta \mathbf{U}_a \right) + \mathcal{L} \mathbf{C}_a, \qquad (4a)$$

$$\partial_t \mathbf{C}_a = \mathbf{A}(\mathbf{U}_a)\, \mathbf{C}_a + \mathbf{C}_a\, (\mathbf{A}(\mathbf{U}_a))^\dagger + \mathbf{Q}, \qquad (4b)$$

$$\partial_t \mathbf{C}_b = \mathbf{A}(\mathbf{U}_a)\, \mathbf{C}_b + \mathbf{C}_b\, (\mathbf{A}(\mathbf{U}_a))^\dagger + \mathbf{Q}. \qquad (4c)$$

The two fields will be considered synchronized if as $t \to \infty$, $\mathbf{C}_b \to \mathbf{C}_a$.

Note first that the coupled system admits the synchronized solution: $\mathbf{C}_b = \mathbf{C}_a$ with $(\mathbf{U}_a, \mathbf{C}_a)$ satisfying Eq. (4a), (4b) of the primary S3T system, which is denoted by subscript a. The question is whether this solution is a stable solution of (4c). The linear (and here also nonlinear) stability of the synchronized solution is determined by the maximum Lyapunov exponent (MLE) of

$$\partial_t \delta\mathbf{C}_b = \mathbf{A}(\mathbf{U}_a)\, \delta\mathbf{C}_b + \delta\mathbf{C}_b (\mathbf{A}(\mathbf{U}_a))^\dagger \; ; \qquad (5)$$

if the MLE is negative then these systems synchronize.

However, we know that the MLE of (5) is at most non-positive because the S3T system has bounded solutions; for if the $\mathbf{A}(\mathbf{U}_a)$ operators produced a positive MLE then $\mathbf{C}_a$ would become unbounded. Actually, if $\mathbf{Q} \neq 0$ in Eq. (4b) the MLE must be negative in order that $\mathbf{C}_a$ not grow as a random walk and only for $\mathbf{Q} = 0$ is the MLE exactly zero. An improved parameterization of the neglected nonlinear term in the perturbation equation would be to augment the dissipation so that no energy was injected into the system by the stochastic parameterization of this conservative nonlinearity; in this case the top MLE is also exactly zero. The first 10 Lyapunov exponents of $A(U_a)$ are shown in Fig. 3 for the case in which system (a) self-sustains with $\mathbf{Q} = 0$. With $\mathbf{Q} = 0$ the MLE is exactly zero and both $\mathbf{C}_a$ and $\mathbf{C}_b$ assume asymptotically the structure of the first Lyapunov vector associated with this zero MLE. However, $\mathbf{C}_a$ and $\mathbf{C}_b$ may differ in amplitude (to the degree the initial state of $\mathbf{C}_b$ projects on the top Lyapunov vector). Therefore it is required in this case to accept the synchronization condition that the perturbation states are synchronized if the normalized covariances converge i.e. if

$$\delta(t) = \left|\left| \frac{\mathbf{C}_a}{||\mathbf{C}_a||} - \frac{\mathbf{C}_b}{||\mathbf{C}_b||} \right|\right| \to 0 \; . \qquad (6)$$

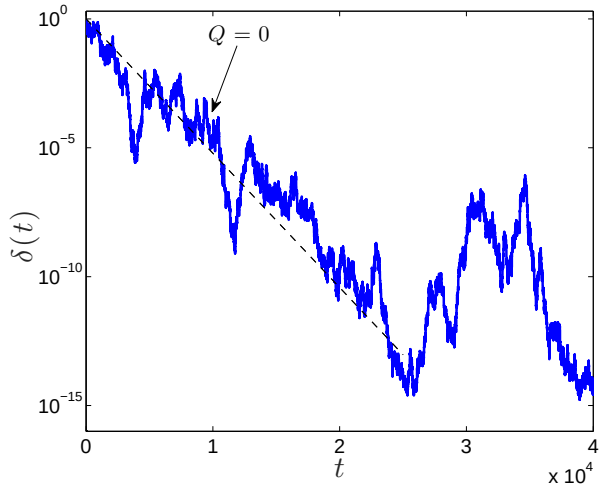

FIG. 4: The approach towards synchronization of two RNL_∞ systems with $\mathbf{Q} = 0$. The decay towards synchronization is measured by $\delta(t) = ||\mathbf{C}_a/||\mathbf{C}_a|| - \mathbf{C}_b/||\mathbf{C}_b||||$, which decays at twice the rate of the second Lyapunov exponents of $\mathbf{A}_k(\mathbf{U})$ which is indicated by the dashed line.

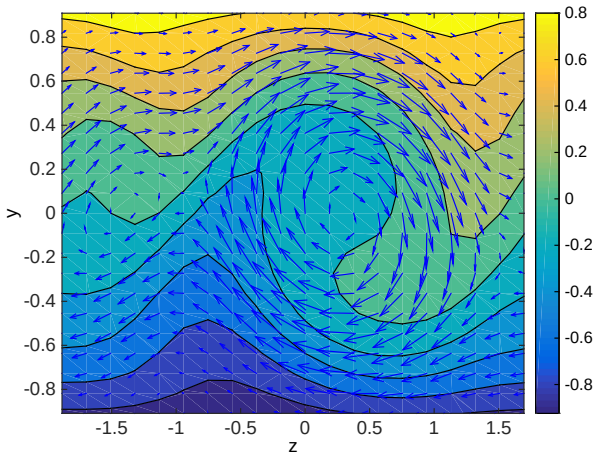

FIG. 5: Snapshot of the contours of the streamwise mean flow U_a and vectors indicating the streamwise mean velocity (V, W). This is for $\mathbf{Q} = 0$ and the S3T system in a self-sustained state.

PERTURBATION DYNAMICS OF S3T TURBULENCE UNDER SYNCHRONIZATION

We demonstrate the synchronization of the eddy covariance $\mathbf{C}_b$ with the covariance $\mathbf{C}_a$ of the RNL (4a), (4b) if $\mathbf{C}_b$ in (4c) is evolving under the influence of the time dependent zonal mean $\mathbf{U}_a$ of (4a) and (4b) with $\mathbf{Q} = 0$. In this experiment $\mathbf{C}_b$ is initialized with a random structure white in energy. From the structure of the equation i.e. the synchronized system (4b) is a linear time dependent equation with the time dependence arising from the essentially stochastically varying $\mathbf{U}_a$ of the S3T turbulence, we expect that asymptotically in time the covariances, $\mathbf{C}$, in these two systems will converge to the rank 1 covariance associated with the first Lyapunov vector of the primary system (system (a)). The time-dependent amplitude of the first Lyapunov vector in the primary system is determined by the dynamics to lie on the turbulent state trajectory. Because the first Lyapunov exponent is zero in the primary system, consistent with it being a component of the the state trajectory, the amplitude in both the primary and synchronized systems are predicted to be statistically steady. However, as discussed in the previous section, while the amplitude of the first Lyapunov vector in the primary system is required by the dynamics to be that of the turbulent equilibrium, in the synchronized system an arbitrary amplitude is attained depending on the projection of the random initial condition on the first Lyapunov structure in this system. Eigenanalysis of $\mathbf{C}_b$ produces the structure of all the remaining Lyapunov vectors that are decaying with time with the Lyapunov exponents shown in Fig. 3 for $\mathbf{Q} = 0$. Consistent with the MLE being zero and with the negative Lyapunov exponents of the remaining Lyapunov vectors in the primary system and the full rank initial covariance in the synchronized system (which was initialized white in energy) approaches being supported by the single Lyapunov structure of the primary system trajectory asymptotically in time. Consistently, the initialized Lyapunov vectors other than the first decay in amplitude in the order of their (negative) Lyapunov exponents, as shown in Fig. 7.

We have verified that turbulence in two S3T systems can be synchronized by coupling only the mean streamwise velocity of the two systems. We now wish to exploit this tool to study perturbation dynamics in S3T turbulence.

STRUCTURE AND DYNAMICS OF THE PERTURBATION FIELD IN S3T TURBULENCE

Consider next the dynamical mechanism maintaining the perturbations. In a similar problem at $R_e = 400$ [13] this dynamical mechanism was found to be the non-normal parametric growth process that is a general attribute of time-dependent dynamical systems [33, 34]. Moreover, it was also shown that the growth process is unrelated to episodic occurrence of notional modal instability in this time-dependent system. In order to further study the dynamical mechanism maintaining turbulence the following experiment is performed: at each instant the normalized perturbation state is projected on the ellipsoid the principal axes of which are in the directions of the eigenvectors of the symmetric matrix $\mathbf{A} + \mathbf{A}'$. By

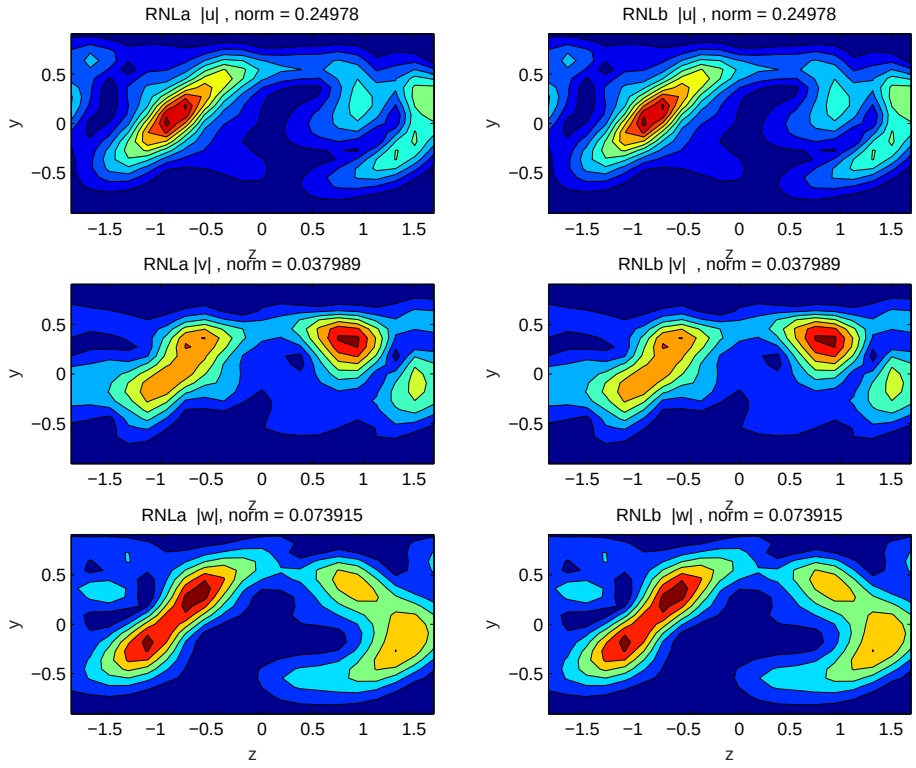

FIG. 6: Contours of the absolute values of the three components of the perturbation velocities of the normalized top singular vector of $\mathbf{C}_a$ of the primary system (a) (left panels) and of the top singular vector of $\mathbf{C}_b$ of the synchronized system (b) (right panels) initialized with a different initial condition. The figure demonstrates that time varying mean streamwise velocity is associated with a unique perturbation state to which initial conditions converge. This experiment shows that synchronization of the normalized structures of the perturbation states in S3T turbulence occurs with only the streamwise mean streak being coupled.

singular value decomposition $\mathbf{USU}' = \mathbf{A} + \mathbf{A}'$ with $\mathbf{U}$ the matrix composed of the instantaneous eigenvectors of $\mathbf{A} + \mathbf{A}'$ arranged in columns and $\mathbf{S}$ is the diagonal matrix of the corresponding eigenvalues. The instantaneous growth rate of perturbation energy is $g(t) = \mathbf{u}'\mathbf{USU}'\mathbf{u}/\mathbf{u}'\mathbf{u}$. Similarly, we can calculate the growth rate of the perturbation energy that would be obtained if the eigenmodes were orthogonal with the same eigenvalues by forming the ellipsoid the principal axes of which correspond to the instantaneous growth rate of the eigenmodes of $\mathbf{A}$ and projecting the normalized state on these eigenmodes. The normalized projections of the perturbation state $\mathbf{u}$ on this ellipsoid are then the instantaneous equivalent normal growth rates i.e. the growth rates that would occur if $\mathbf{A}$ were a normal matrix with these eigenvalues. The equivalent normal energy growth rate is given by $h(t) = \mathbf{u}'\mathbf{EDE}^{-1}\mathbf{u}/(\mathbf{u}'\mathbf{E}^{-1'}\mathbf{E}^{-1}\mathbf{u})$ where $\mathbf{E}$ is the matrix consisting of the instantaneous eigenvectors of $\mathbf{A}$ arranged in columns and $\mathbf{D}$ is the diagonal matrix of twice the associated modal growth rates of the modes.

The probability distribution function (PDF) of the eigenvalues of $\mathbf{A} + \mathbf{A}'$, which correspond to the axes of the instantaneous growth rate ellipsoid, and the PDF of the eigenvalues of $\mathbf{A}$, which correspond to the axes of the modal growth rate ellipsoid, are shown for a self-sustaining turbulent state over a time interval $\tau = 5000$ in Fig. 8. The instantaneous growth rate of the perturbation state is determined by its projection on the instantaneous growth rate ellipsoid. This projection varies in time due to both the time dependence of the state vector and the time dependence of the growth rate ellipsoid. The distributions of the resulting projections for a turbulent simulation over a time period $\tau = 5000$ is shown in Fig. 9. This figure contains information on both the extent of the growth rates sampled by the state vector as well as the frequency with which these values are sampled. The state vector fails to explore the extremities of the growth rate ellipsoid with most projections being confined around zero growth rate. The information in Fig. 9 is summarized by the cumulative distribution function (CDF) of the square projections of the state on

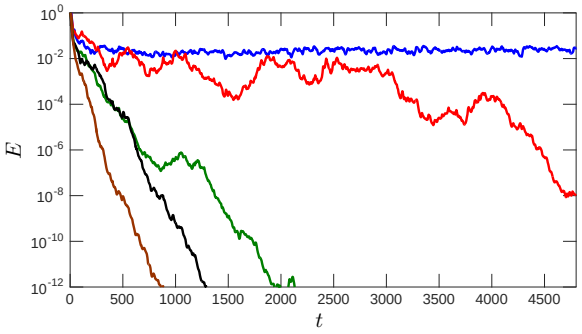

FIG. 7: Evolution of the energy of the first 5 Lyapunov vectors of the perturbation covariance dynamics which has been synchronized with the mean flow of the turbulent S3T system (a) and initialized white in energy. The streamwise wavenumber of all the Lyapunov vectors is $k = 2\pi/L_x$ so the individual members of the orthogonal set of Lyapunov vectors differ only in their $y - z$ structure. The MLE associated with the first Lyapunov vector is zero consistent with it constituting a component of the statistical steady state. Except for this first Lyapunov vector, the remaining vectors decay at the rate of their negative Lyapunov exponents. However, the second Lyapunov vector has a small negative Lyapunov exponent and exhibits large excursions associated with the time dependence of the dynamical operator. The channel has $L_x = 1.75\pi$, $l_z = 1.2\pi$ and $R = 600$.

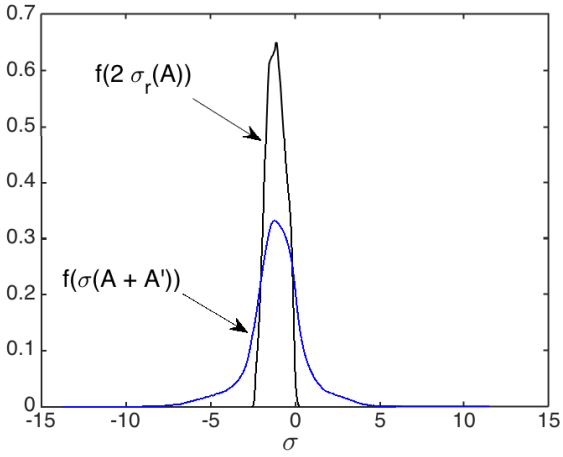

FIG. 8: The PDF of the eigenvalues of the instantaneous perturbation operators $\mathbf{A} + \mathbf{A}'$ and of twice the real part of the instantaneous eigenvalues of $\mathbf{A}$ for mean states that occur over a time period $\tau = 5000$. The mean growth rate for both cases is -1.14, the standard deviation of $\sigma(\mathbf{A} + \mathbf{A}')$ is 1.6 and the range in the specific simulations is $[-18.2, 16.2]$, while the standard deviation of $2\sigma_r(\mathbf{A})$ is 0.5 and the range is $[-2.9, 0.4]$. The eigenvalues of $\mathbf{A} + \mathbf{A}'$ correspond to the axes of the growth rate ellipsoid. The extrema of these possible growth rates exceed that of the instantaneous eigenfunction growth rates as expected for a non-normal system. Remarkably, only very small positive modal growth rates occur suggesting that the system is constrained to limit the extent of modal instability.

the principal axes of the growth rate ellipsoid shown in Fig. 10. This CDF is obtained from Fig. 9 by forming $F(\sigma) = \int_{-\infty}^{\sigma} \delta(\sigma' - \sigma_i)|\alpha_i|^2 d\sigma' / \int_{-\infty}^{\infty} \delta(\sigma' - \sigma_i)|\alpha_i|^2 d\sigma'$ in which each of the points in Fig. 9 is a sample $(\sigma_i, |\alpha_i|^2)$. The smooth derivative of the CDF, also shown in Fig. 10, is the PDF of the perturbation state projections, $|\alpha(\sigma)|^2$, on the energy growth rate, σ. Despite the wide distribution of available growth rates (cf. Fig. 8) the self-sustained state projects on growth rates narrowly centered around zero with values primarily in the interval $[-1, 1]$. The mean growth rate of the state, $\lambda = \int_{-\infty}^{\infty} \sigma f(\sigma) d\sigma$, vanishes consistent with the perturbation being a component of the statistically stable turbulent state trajectory, i.e. the state trajectory, corresponding to the first Lyapunov vector (LV1), has been adjusted through its interaction with the mean flow to have zero Lyapunov exponent, which is the MLE of the perturbation dynamics. An equivalent diagnostic, the growth rate PDF, is more easily obtained directly from the time series of the growth rates of the individual Lyapunov vectors. This PDF is shown for LV1, and also for the decaying Lyapunov vectors LV2, LV3, and LV10, in Fig. 11 in which it can be seen that, although it is decaying asymptotically, LV2 is similar to LV1 in its dynamics with only a small negative mean growth rate. Because of the stochastic time dependence of the dynamics of $\mathbf{A}$, the nearly zero Lyapunov exponent of LV2 results in its undergoing large excursions in energy as it decays (cf. Fig. 7) Such large excursions are characteristic of the energetics of stochastic dynamical systems with multiplicative noise[34–36] and these excursions will be shown to have important implications for the dynamics of RNL turbulence when a stochastic parameterization of the third cumulant is included in the model. In fact, it is not just LV1 and LV2 that have similar dynamics: all of the Lyapunov vectors are similarly supported by their essentially stochastic in time projection on the growth ellipse. Given that these structures in sum account for the perturbation energy it follows that the mechanism maintaining the perturbation energy of RNL turbulence is parametric interaction with the mean flow and the structure of the turbulence is primarily determined by the structure of the LV's. We will further explore consequences of this observation but first we wish to examine the dynamics of the parametric mechanism in more detail.

The linear perturbation dynamics is strongly time dependent with the dynamical operator $\mathbf{A}$ and associated growth rate ellipsoid adjusted by the dynamics of the in-

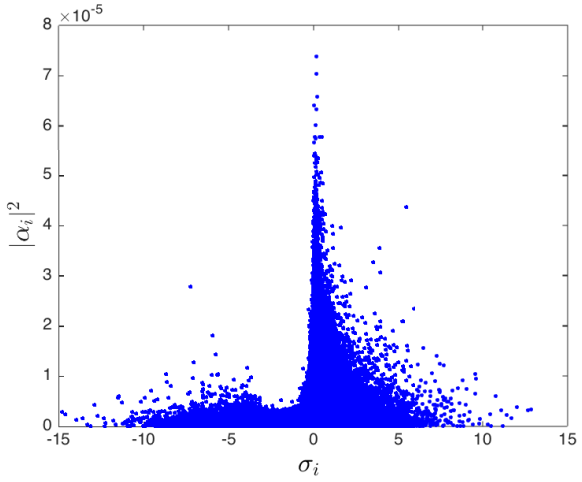

FIG. 9: Instantaneous projections of the normalized state vector on the axes of the ellipsoid of energy growth rate. Each point has coordinates $(\sigma_i, |\alpha_i|^2)$ where σ_i is the i-th eigenvalue of $\mathbf{A} + \mathbf{A}'$ and $|\alpha_i|^2$ is the square amplitude of the projection of the normalized state on this principal axis. This figure reveals both the magnitude of the projection of the state on the growth rate axes and, by the density of the points, the frequency of the occurrence of each growth rate.

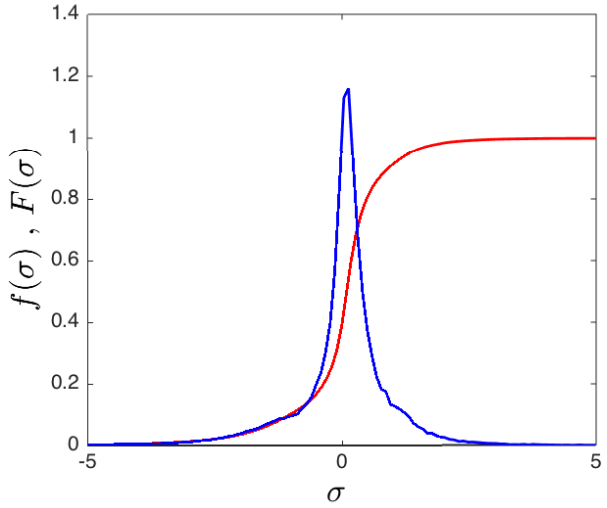

FIG. 10: Cumulative distribution function (CDF) of the square projection of the normalized state on the axes of the growth rate ellipsoid (red). The smooth derivative of the CDF, $f(\sigma)$, (shown in blue), is the PDF of the perturbation state projections $|\alpha(\sigma)|^2$ on the energy growth rate σ.

teraction between the mean flow and the perturbation field to exhibit large excursions in growth rate on short time scales. However, as shown in Fig. 8, the system adjusts to support only weak instantaneous inflectional instability. A time series of the maximum instantaneous modal energy growth rate, σ_r, is shown in Fig. 12. The mean of the maximum growth rate is only 0.045 and the growth rate varies rapidly. Also shown is the time series of the normalized fluctuations of the maximum streak amplitude $U_s^m \equiv \max(U_s(y,z)) - \min(U_s(y,z))$ together with normalized fluctuations of the maximum growth rate, $\sigma_r' = \sigma_r - \langle\sigma_r\rangle$. The streak amplitude and the maximum instability growth rate are substantially correlated consistent with inflectional instability of the streak. However, while the state dynamics adjusts to consistently exhibit a small and rapidly varying instantaneous modal instability, this instability is not itself responsible for sustaining the perturbation variance. Shown in Fig. 13 is the autocorrelation and crosscorrelation of streak amplitude and maximum modal growth rate. The streak and modal instability are correlated with essentially zero lag, as expected for inflectional mode instability, but both of these quantities decorrelate in approximately ten time units which is inconsistent with emergence of the modal instability which has an approximatel e-fold time of 20 (cf. Fig. 12). That modal growth does not account for maintenance of the perturbation variance is confirmed in Fig. 14 in which is shown a time series of the energy growth rate of the perturbation field together with the energy growth rate that would occur if the state were projected on the eigenvectors of the instantaneous operator A and each advanced at the rate of the corresponding real part of the eigenvalue of A is also shown. Although it can be seen from Fig. 12 that the instantaneous mean flow is nearly always modally unstable, it can be seen from Fig. 14 that the contribution to maintaining the Lyapunov vector of the perturbation trajectory arising from modal growth is almost always negative with the time mean value of the equivalent normal contribution to the energy of the perturbation field being decay at rate -0.7. In contrast, the non-normal parametric mechanism produces robust excursions of both positive and negative growth rate due to rapidly varying projections of the perturbation state on the equally rapidly varying directions of growth associated with variation of the streak (cf. Fig. 13). These positive and negative contributions average of necessity to zero consistent with the associated Lyapunov vector being adjusted through interaction with the streak to be a component of the system trajectory (cf. Fig. 14). This parametric growth mechanism is a general attribute of stochastic dynamical systems which are necessarily non-normal with measure zero exception. This result arises from the concatenation of non-normal growth events which are sustained by the convexity of the exponential propagator of the dynamics [33, 34]. A characteristic property of this stochastic parametric growth process is parametric variation of the system on intermediate time scales. This is because the convexity of the exponential vanishes at short time scales

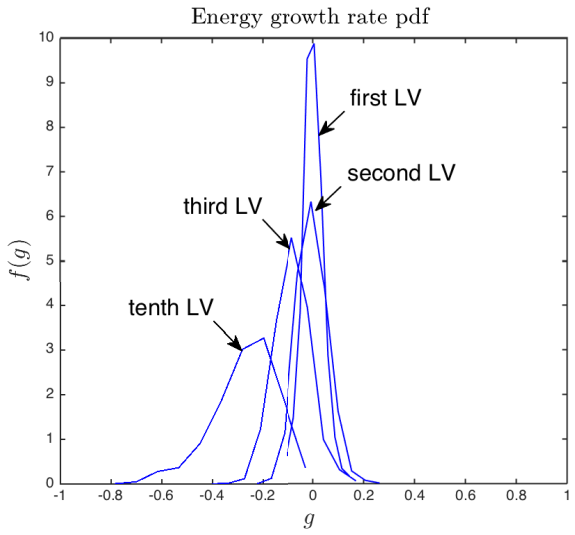

FIG. 11: The probability distribution of the instantaneous growth rates of LV1, LV2, LV3, LV10. LV2 is only slightly decaying and has a narrowly confined distribution similar to that of LV1 while the LV3 and LV10 decay strongly and sample a wider range of growth rates.

and the transient perturbation growth vanishes at long time scales. Consistently, the fluctuations of the streak and the fluctuation in the growth rate of LV1 fit a red noise process as shown in Fig. 15. Consistent with the stochastic parametric growth mechanism, the correlation time of this red noise process, $\tau = 5.0$, is short compared to the modal growth time scale (cf. Fig. 12).

In Fig. 7 the time series corresponding to LV2, which has negative Lyapunov exponent, is shown. It can be seen that this Lyapunov vector has nearly the same energetic interaction with the fluctuating streak as does the trajectory Lyapunov vector, LV1, and it just fails to attain neutrality (cf. Fig. 11). This observation invites the conjecture that in the presence of stochastic parameterization of the neglected perturbation-perturbation nonlinearity the remaining Lyapunov vectors, which are asymptotically stable in the absence of excitation, would be maintained at significant amplitude, primarily by the parametric growth process. If so then the energetics maintaining the perturbation variance would be identified to be primarily the parametric growth process, the structure of the perturbation variance to be primarily that of the Lyapunov vectors and these structures to be ordered in variance in approximate inverse order with the decay rate of the Lyapunov vectors. In order to investigate these predictions, an additive noise white in energy and time is include in the primary and synchronized systems. Under this parameterization of the neglected perturbation-perturbation interactions, the primary system maintains a set of structures each of which we refer to as a stochastically forced Lyapunov vector (SFLV). The first of these is equal to LV1 asymptotically for vanishing stochastic excitation but increasingly diverges as the parameterization increases in amplitude. The remaining SFLV's are associated with the damped LV's but become under this parameterization statistically steady at finite energy, being maintained by the stochastic parameterization. We wish to test the conjecture that the statistically steady state of these structures, including that of SFLV1, which remains primarily responsible for maintaining the SSP, are similarly maintained by parametric growth and to what extent the SFLV's retain the structure of their associated unforced LV. To do so we perform a simulation in which a stochastic parameterization for the third cumulant is included with amplitudes equal to that which would maintain perturbation variance 16%, 1%, and 1/16% of the energy of the mean Couette flow when used to force the Couette flow. Time series of the energy of the SFLV's are obtained as the eigenvalues of the perturbation covariance matrix. These time series are shown as the amplitude of the forcing covariance ϵQ is varied in Fig. 16. The stochastic forcing covariance matrix has been normalized so that unit value corresponds to the parameterized excitation that would maintain variance 1% of the Couette flow energy when introduced into the dynamics of the Couette flow. Values $\epsilon = 16, 1, 1/16$ are chosen for the forcing amplitude in order to bracket the approximate total perturbation variance observed in DNS. The variance maintained by these values of ϵ applied to Couette flow are also indicated in Fig. 16.

Note first that there is continuity in the amplitude of the SFLV's as the amplitude of the forcing is increased indicating that the LV dynamics retains a strong influence on the perturbation variance even in the presence of strong forcing. A revelatory characteristic of the dominance of the parametric mechanism in the perturbation dynamics is the covariance of the amplitude of the SFLV's indicating that the mean flow is producing a common influence on their amplitude despite the orthogonality of these structures. The primary structure, SFLV1, assumes control of the SSP for $\epsilon = 1/16\%$ while at the highest forcing level $\epsilon = 16\%$ the SSP is significantly affected by the SFLV's other than SFLV1. At the intermediate value $\epsilon = 1\%$ SFLV1, which is associated with the nearly neutral LV1 and which as a result undergoes large fluctuations in response to the stochastic variations of $\mathbf{A}$, episodically obtains sufficient amplitude to effect the SSP.

The total perturbation energy can be partitioned into active and passive components by separating the perturbation that is primarily associated with maintaining the SSP, SFLV1, and the remaining spectrum. A time series of the total perturbation energy and of the total perturbation energy minus the energy of SFLV1 is shown in Fig. 16 for $\epsilon = 16, 1, 1/16$. Also shown is the energy that would be maintained at each ϵ if the mean turbu-

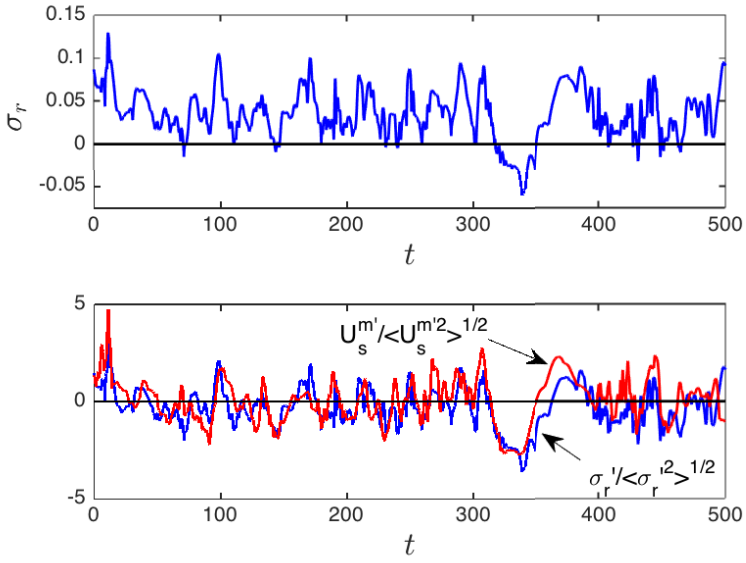

FIG. 12: Top panel: The maximum modal growth rate of $\mathbf{A}(U)$ over a typical interval taken from a time series of length 2000. The mean of the maximum growth rate over the entire time series is 0.045 and the range is $[-0.06, 0.135]$. Bottom panel: Corresponding time series of the normalized fluctuations of the maximum growth rate, $\sigma_r' = \sigma_r - < \sigma_r >$, and of the normalized fluctuations of the maximum streak amplitude $U_s^m \equiv \max(U_s(y,z)) - \min(U_s(y,z))$. The streak amplitude and the maximum instability growth rate are correlated with correlation coefficient $r = 0.4$ consistent with inflectional instability of the streak. However, while the state is tightly constrained to exhibit small but consistent instantaneous modal instability, this instability is not responsible for sustaining the perturbation variance.

lent flow profile were stochastically forced. This allows an estimate of the contribution to the perturbation energy arising from the time dependence of $\mathbf{A}$ to made. From this figure it is clear that the perturbation energy and variance is tightly regulated at strong forcing indicative of a strong upper bound on the perturbation energy. Also, the time dependence of $\mathbf{A}$ and by implication the parametric growth process dominates the perturbation energetics.

Turning now to study the structure of the perturbation field, we first project the perturbation field on the SFLV's. The projection of the state on this time dependent orthogonal basis measures the extent to which the perturbation energy is concentrated in the structures of the SFLV's. Shown in Fig. 17 is the mean projection for $\epsilon = 16, 1, 1/16$. Nearly all of the perturbation energy resides in the first ten SFLV's and for light to moderate forcing nearly all in SFLV1. This result shows that the structure of the perturbation field is determined primarily by interaction with the mean flow through the stochastic parametric growth process. If we go back to the structure of the LV's, which are determined only by the SSP in the absence of forcing, the projection is also good. In Fig. 18 is shown the projection coefficients of the unitary basis of the SFLV's on the corresponding LV unitary basis. We see from this figure that the first two LV's can explain most of the variance in the SFLV's of a stochastically forced RNL and that even the higher SFLV's, which explain little variance, project tightly around their corresponding LV.

MECHANISM REGULATING THE STATISTICAL MEAN STATE OF RNL TURBULENCE

We turn next to study of the mechanism by which the state of RNL_∞ turbulence is regulated to its observed statistical mean. The observation that the streak is constrained to be marginally unstable (cf. Fig. 8 and Fig. 12) suggests that the regulation of the turbulent state may be associated with an adjustment to marginal streak stability [13]. In Fig. 19 is shown the autocorrelation of the streak energy ϵ_s, and the perturbation Reynolds stress divergence term in the streak energy equation, $\dot{\epsilon}_F$ together with the cross correlation of these quantities $< \dot{\epsilon}(t+\tau)\epsilon_s(t) >$. The cross correlation between ϵ_s and $\dot{\epsilon}_F$ reveals that these quantities are closely correlated with only a $\tau = 1.8$ lead of the streak energy over the Reynolds stress term. The Reynolds stress term in the streak energy equation is always negative so this strong correlation at short lead corresponds to a rapidly acting regulation of the streak energy by the Reynolds stress. The small

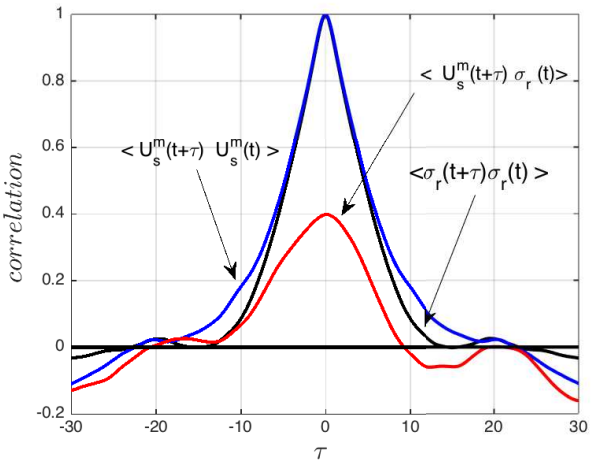

FIG. 13: Autocorrelation of streak amplitude, $U_s^m \equiv \max(U_s(y,z)) - \min(U_s(y,z))$, and maximum modal growth rate, σ_r. Also shown is the cross correlation of these quantities. The streak and modal instability are highly correlated as expected for inflectional mode instability but both of these quantities decorrelate in approximately ten time units which is too short a time for the modal instability to emerge given its typical time scale for growth of approximately 20 time units (cf. Fig. 12).

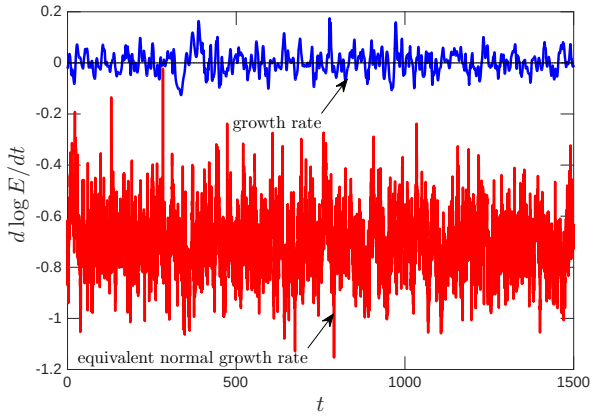

FIG. 14: Time series of the energy growth rate of the synchronized perturbation field (blue). This growth rate is equal to the projection of the normalized state on $A + A^\dagger$ and its mean value is 0 consistent with its being the perturbation component of the state trajectory. Energy growth rate that would occur if the state were projected on the eigenvectors of instantaneous operator A and each advanced at the rate of the corresponding real part of the eigenvalue of A is also shown (red). The mean value of this equivalent normal growth rate is -0.7. We conclude that while the instantaneous mean states are often modally unstable (cf. Fig. 12) the perturbation state does not project sufficiently on the instabilities to account for its growth. This result demonstrates that the perturbation field is sustained by the parametric non-normal growth process rather than by modal instability.

lead time indicates that transient growth on the advective time scale rather than instability growth on the much longer instability time scale ($1/\sigma_{\max} = 20$ is involved in this regulation of the streak energy (cf. Fig. 12).

In Fig. 20 is shown the various energetic terms that contribute in the maintenance of the streak energy. The rapid response of the Reynolds stress to increases in streak amplitude indicates a tight coupling between these quantities. These results are summarized in Fig. 21 in which the tight balance between the lift up term building the streak and the Reynolds stress term damping it is shown. This tight coupling and the availability of very rapidly growing energy damping fluxes associated with streak energy increase explains the robustness of the turbulent state in RNL: the streak grows relentlessly by lift-up due to the roll forcing by the perturbations resulting from the parametric instability of LV1 which would cause the streak amplitude to run away if it were not for the even stronger transient growth of the adjoint modes associated with incipient streak instability [13] which strongly damp the streak energy producing a tightly controlled equilibrium statistical state.

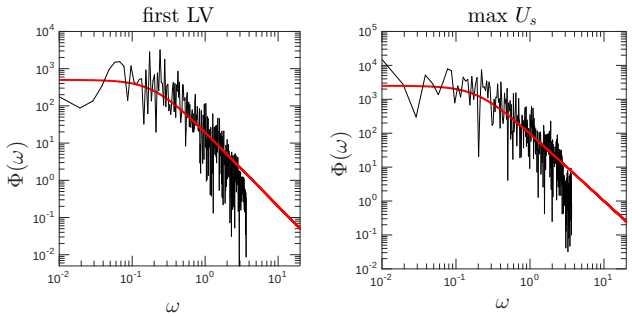

FIG. 15: Spectral density of the growth rate of the first Lyapunov vector (LV) and of the maximum streak velocity time series and their fit to the Lorentzian $625\tau^{-2}/((\omega\tau)^2+1)$ and $100U_{\max}\tau^2/((\omega\tau)^2+1)$ with $\tau = 5.0$, respectively. This graph shows that the instantaneous growth rate of the perturbations are a red noise process and that the streak fluctuations follow the same red noise process.

Conclusion

The S3T system is a statistical state dynamics closed at second order that has highly simplified dynamics and

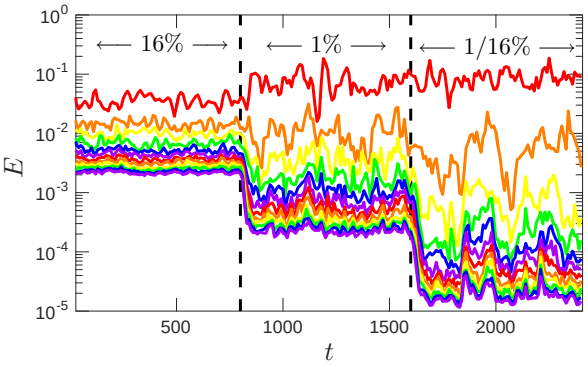

FIG. 16: Time series of the energy of the stochastically forced Lyapunov vectors (SFLV's) for stochastic forcing covariance ϵQ with amplitudes $\epsilon = 16, 1, 1/16$ where $\epsilon = 1$ would maintain perturbation energy which is 1% of the energy of the laminar Couette flow. The dashed horizontal lines indicate this mean energy maintained by this forcing if applied to the laminar Couette flow. As the amplitude of the forcing is reduced fewer SFLV's are involved in the regulation of the turbulence. The SFLV's are correlated indicating interaction with the non-normal time dependent operator $A(U)$. The second SFLV, which is associated with the nearly neutral LV2, exhibits large excursions.

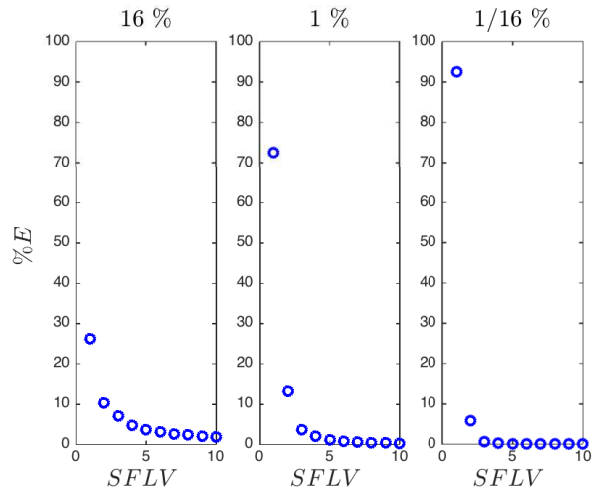

FIG. 17: Percentage of the perturbation energy explained by the SFLV's. Shown are results for stochastic excitation amplitude that would sustain mean perturbation energy 16%, 1% and 1/16% of the energy of the laminar Couette flow.

naturally maintains a turbulent state with highly reduced support in streamwise wavenumber so that S3T turbulence is dynamically and computationally greatly simplified. Even so, S3T system turbulence is in many aspects realistic and in particular it supports a realistic SSP. In this work we have exploited the simplicity of the SSP in S3T turbulence to study the mechanisms underlying the maintenance of turbulence in this system at its observed statistical equilibrium. The mechanism maintaining the turbulence is found to be the stochastic parametric growth process and consistently the resulting structure of the perturbation state is that of the first Lyapunov vector supported by the time-dependent streak. It is also verified that under a stochastic parameterization closure for the third cumulant the structure of the perturbation field remains close to the support of the LV1 augmented by a small number of additional LV's. This result identifies the structure of the turbulence perturbations with the LV's supported by the stochastic parametric growth process. Finally, the mechanism by which the statistical mean state is determined in S3T turbulence was identified to be the tight balance between robust streak growth by lift-up due to the roll forcing by the perturbations which in turn results from the parametric instability of LV1 and the even stronger damping resulting from transient growth of the adjoint modes which arise as the streak grows in association with the strong damping of streak amplitude arising from ever very slight streak instability [13]. These competing processes of robust streak growth opposed by strong damping produce a tightly controlled equilibrium statistical state.

The advantage of the RNL system is the facility with which the mechanism of RNL turbulence can be studied. The challenge is now to use these results to understand NS turbulence.

Appendix

The first two equal time cumulants c^i of flow component $\psi_i(\mathbf{x}, t)$ at position $\mathbf{x}$ and time t and c^{ij}_{12} of the flow field components $\psi_i(\mathbf{x}_1, t)$ and $\psi_i(\mathbf{x}_2, t)$ at positions $\mathbf{x}_1$ and $\mathbf{x}_2$ respectively are defined by:

$$c^i(\mathbf{x}, t) \equiv \langle \psi_i(\vec{x}, t) \rangle \ , \tag{A.7a}$$

$$c^{ij}_{12} \equiv c^{ij}(\mathbf{x}_1, \mathbf{x}_2, t) \equiv \left\langle \psi'_i(\mathbf{x}_1, t) \psi'_j(\mathbf{x}_2, t) \right\rangle , \tag{A.7b}$$

with $\psi'_i(\mathbf{x}, t)$ the deviation form the mean i.e. $\psi'_i(\mathbf{x}, t) \equiv \psi_i(\mathbf{x}, t) - \langle \psi_i(\mathbf{x}, t) \rangle$. By $\langle \cdot \rangle$ we denote an ensemble average and we will make the ergodic assumption that this is equal to the streamwise average of the flow at each time instant with the streamwise averaging operation denoted by an overbar. If the full cumulant expansion is truncated at second order and all cumulants higher than the second are disregarded we obtain a closed dynamics for the evolution of the first two cumulants of the flow, which is referred to as the second order cumulant expansion (CE2) approximation to the full SSD [18, 32]. If the higher order cumulants are parameterized as a Gaussian random process with second order cumulant q^{ij}_{12} we obtain the approximation to the SSD dynamics of the Stochastic Structural Stability Theory (S3T) [13, 14]. Despite the

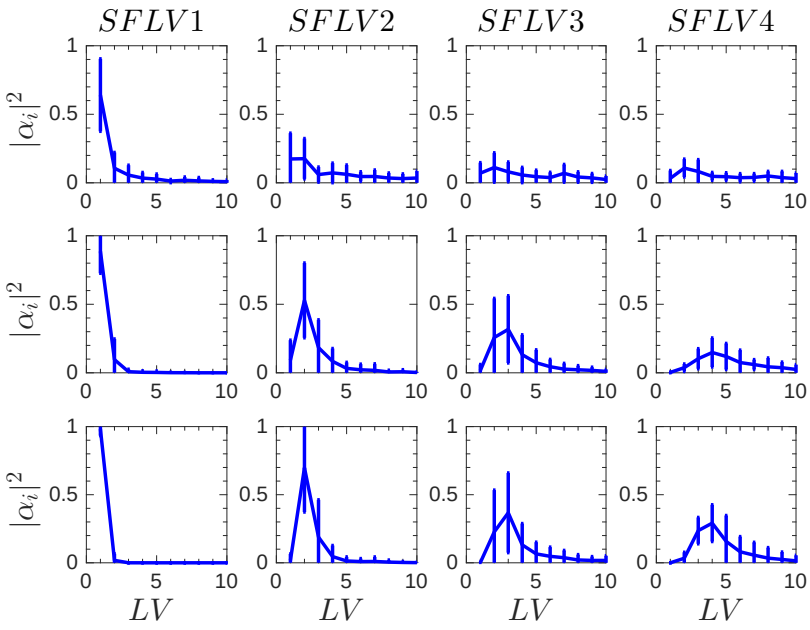

FIG. 18: Projection coefficients of the unitary basis of the SFLV's on the coresponding LV unitary basis. Shown are projections for stochastic excitation amplitudes that sustains perturbation energy 16% (top row), 1% (middle row) and 1/16% (bottom row) of the laminar Couette flow energy. This figure shows that the LV structure persists under stochastic forcing and that the first two Lyapunov vectors can explain most of the variance in a stochastically forced RNL.

severity of the approximation of keeping only two cumulants in the CE2 and S3T dynamics, the turbulent state of CE2 and S3T dynamics closely parallels Navier-Stokes turbulence [23, 24, 37].

Having identified the ensemble averages with streamwise averages the equations for the evolution of the first cumulants or the streamwise mean flow, are:

$$\partial_t \mathbf{U} = \mathbf{P}_L \left(-\mathbf{U}\cdot\nabla\mathbf{U} + \frac{1}{R}\Delta\mathbf{U} - \langle \mathbf{u}'\cdot\nabla\mathbf{u}'\rangle \right) \tag{A.8}$$

The term $\mathbf{P}_L(\langle -\mathbf{u}'\cdot\nabla\mathbf{u}'\rangle)$ is the ensemble mean Reynolds stress divergence which depends linearly on the second order velocity cumulants $\mathbf{C}_{12} = \langle \mathbf{u}'_1\cdot\nabla\mathbf{u}'_2\rangle$, and is written as $\mathcal{L}\mathbf{C}$. The first cumulant equation thus becomes:

$$\partial_t \mathbf{U} = \mathbf{P}_L \left(-\mathbf{U}\cdot\nabla\mathbf{U} + \frac{1}{R}\Delta\mathbf{U} \right) + \mathcal{L}\mathbf{C} \ . \tag{A.9}$$

The second cumulant equation is obtained by differentiating $\mathbf{C}_{12} = \langle \mathbf{u}'_1\cdot\nabla\mathbf{u}'_2\rangle$ with respect to time and using the equations governing the deviation velocities

$$\begin{aligned}\partial_t \mathbf{u}' = \mathbf{P}_L &\left(-\mathbf{U}\cdot\nabla\mathbf{u}' - \mathbf{u}'\cdot\nabla\mathbf{U} + \frac{1}{R}\Delta\mathbf{u}' \right) \\ &- \mathbf{P}_L \left(\mathbf{u}'\cdot\nabla\mathbf{u}' - \langle \mathbf{u}'\cdot\nabla\mathbf{u}'\rangle \right) \ ,\end{aligned} \tag{A.10}$$

to obtain

$$\partial_t \mathbf{C}_{12} = \left(\mathbf{A}(\mathbf{U}_1) + \mathbf{A}(\mathbf{U}_2)\right)\mathbf{C}_{12} + \mathbf{G}_{\mathbf{123}} \tag{A.11}$$

The term $\mathbf{G}$ is proportional to the third cumulant. In S3T $\mathbf{G}$ is either neglected or parameterized as the spatial covariance of a temporally white noise process. In this work we will set $G = 0$. The term $\mathbf{A}(\mathbf{U}_1)\mathbf{C}_{12}$ is bilinear in $\mathbf{U}$ and $\mathbf{C}_{12}$ and denotes

$$\mathbf{P}_L \left(\left\langle \left(-\mathbf{U}_\mathbf{1}\cdot\nabla_1\mathbf{u}'_1 - \mathbf{u}'_1\cdot\nabla_1\mathbf{U}_\mathbf{1} + \frac{1}{R}\Delta_1\mathbf{u}'_1 \right)\mathbf{u}'_2 \right\rangle \right) \ , \tag{A.12}$$

with the subscript 1 or 2 indicating that the functions are evaluated at position 1 or 2 and the differential operators with subscript 1 or 2 operate on the variable at the corresponding position. By exchanging 1 to 2 we obtain the definition of $\mathbf{A}(\mathbf{U}_2)\mathbf{C}_{12}$.

Consequently the RNL system is :

$$\partial_t \mathbf{U} = \mathbf{P}_L \left(-\mathbf{U}\cdot\nabla\mathbf{U} + \frac{1}{R}\Delta\mathbf{U} \right) + \mathcal{L}\mathbf{C} \ , \tag{A.13a}$$

$$\partial_t \mathbf{C}_{12} = \left(\mathbf{A}(\mathbf{U}_1) + \mathbf{A}(\mathbf{U}_2)\right)\mathbf{C}_{12} \ , \tag{A.13b}$$

Because the ensemble averaging has been interpreted as streamwise average the covariance equations are invariant under translations in the streamwise direction and as result if the initial state covariance is a homoge-

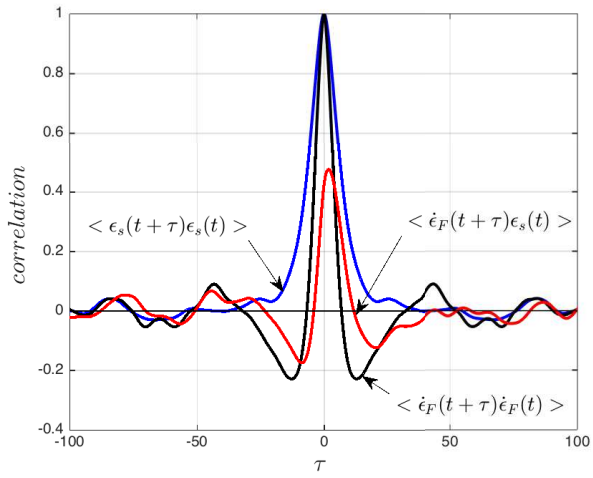

FIG. 19: Autocorrelation of the streak energy ϵ_s, and the perturbation Reynolds stress divergence term in the streak energy equation, $\dot{\epsilon}_F$. Shown also is the cross correlation of these quantities $< \dot{\epsilon}(t+\tau)\epsilon_s(t) >$. The cross correlation between ϵ_s and $\dot{\epsilon}_F$ reveals that these quantities are closely correlated with only a $\tau = 1.8$ lead of the streak energy over the Reynolds stress term.

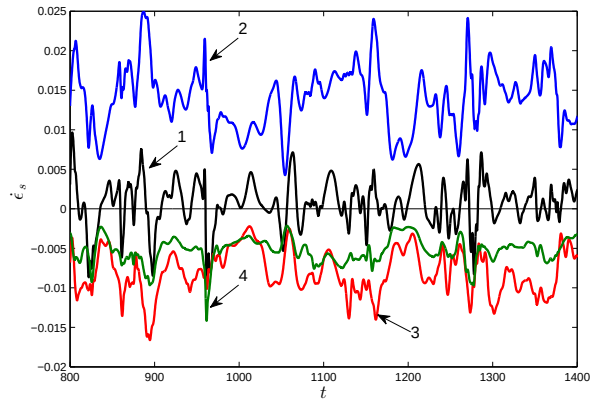

FIG. 20: Time series of the time rate of change in streak energy $\dot{\epsilon}_s$ in an RNL simulation (curve 1). Indicated contributions are mean advection (curve 2 with primary contribution from the lift up term $-\int U_s V \partial_y U dydz$), perturbation Reynolds stress (curve 3 with primary contribution from the spanwise component of the Reynolds stress divergence $-\int U_s \partial_z \overline{(uw)} dydz$) and from the dissipation (curve 4).

neous function of x it will remain homogeneous in x and can be Fourier expanded as $\mathbf{C}(x_1 - x_2, y_1, y_2, z_1, z_2, t)) = \sum_k \mathbf{C}_k(y_1, y_2, z_1, z_2, t) e^{ik(x_1 - x_2)}$. The covariance equation (A.15b) decompose to separate equations for each Fourier component $\mathbf{C}_k$, each of the form:

$$\partial_t \mathbf{C}_{k12} = \left(\mathbf{A}_k(\mathbf{U}_1) + \mathbf{A}_k(\mathbf{U}_2)\right) \mathbf{C}_{k12} \ , \qquad \text{(A.14)}$$

where $\mathbf{A}_k(\mathbf{U})$ is the operator $\mathbf{A}(\mathbf{U})$ in which we have made the substitution $\partial_x \to ik$. Similarly for the operator $\mathcal{L}_k$.

To obtain numerical realizations of the RNL dynamics we discretize the equations (A.15) and the equations assume the matrix form:

$$\partial_t \mathbf{U} = \mathbf{P}_L \left(-\mathbf{U} \cdot \nabla \mathbf{U} + \frac{1}{R} \Delta \mathbf{U} \right) + \sum_k \mathcal{L}_k \mathbf{C}_k \ , \qquad \text{(A.15a)}$$

$$\partial_t \mathbf{C}_k = \mathbf{A}_k(\mathbf{U}) \mathbf{C}_k + \mathbf{C}_k \mathbf{A}_k(\mathbf{U})^\dagger, \qquad \text{(A.15b)}$$

where $\dagger$ denotes the Hermitian transpose. A concrete representation of the operators can be found in Ref. [13].

This work was initiated during the 2013 First Multiflow Summer Workshop at the Universidad Politécnica de Madrid with financial support from the Multiflow Program of the European Research Council. We would like to thank Prof. Javier Jiménez, Prof. Dennice Gayme, Dr. Vaughan Thomas, Dr. Adrian Lozano-Durán and Dr. Navid Constantinou for useful comments and fruitful discussions. Brian Farrell was partially supported by NSF AGS-1246929.

* pjioannou@phys.uoa.gr

[1] S. J. Kline, W. C. Reynolds, F. A. Schraub, and P. W. Runstadler, J. Fluid Mech. **30**, 741 (1967).
[2] K. M. Butler and B. F. Farrell, Phys. Fluids **4**, 1637 (1992).
[3] S. C. Reddy and D. S. Henningson, J. Fluid Mech. **252**, 209 (1993).
[4] M. T. Landahl, J. Fluid Mech. **98**, 243 (1980).
[5] J. D. Swearingen and R. F. Blackwelder, J. Fluid Mech. **182**, 255 (1987).
[6] H. P. Bakewell Jr. and L. Lumley, Phys. Fluids **10**, 1880 (1967).
[7] F. Waleffe, Stud. Appl. Math. **95**, 319 (1995).
[8] K. Hamilton, J. Kim, and F. Waleffe, J. Fluid Mech. **287**, 317 (1995).
[9] F. Waleffe, Phys. Fluids **9**, 883 (1997).
[10] P. Hall and S. Sherwin, J. Fluid Mech. **661**, 178 (2010).
[11] W. Schoppa and F. Hussain, J. Fluid Mech. **453**, 57 (2002).
[12] B. F. Farrell and P. J. Ioannou, Phys. Fluids A **5**, 1390 (1993).
[13] B. F. Farrell and P. J. Ioannou, J. Fluid Mech. **708**, 149 (2012).
[14] B. F. Farrell and P. J. Ioannou, J. Atmos. Sci. **60**, 2101 (2003).
[15] B. F. Farrell and P. J. Ioannou, Phys. Fluids A **5**, 2600 (1993).
[16] T. DelSole and B. F. Farrell, J. Atmos. Sci. **53**, 1781 (1996).
[17] T. DelSole, Surv. Geophys. **25**, 107 (2004).
[18] J. B. Marston, E. Conover, and T. Schneider, J. Atmos. Sci. **65**, 1955 (2008).
[19] S. M. Tobias, K. Dagon, and J. B. Marston, Astrophys.

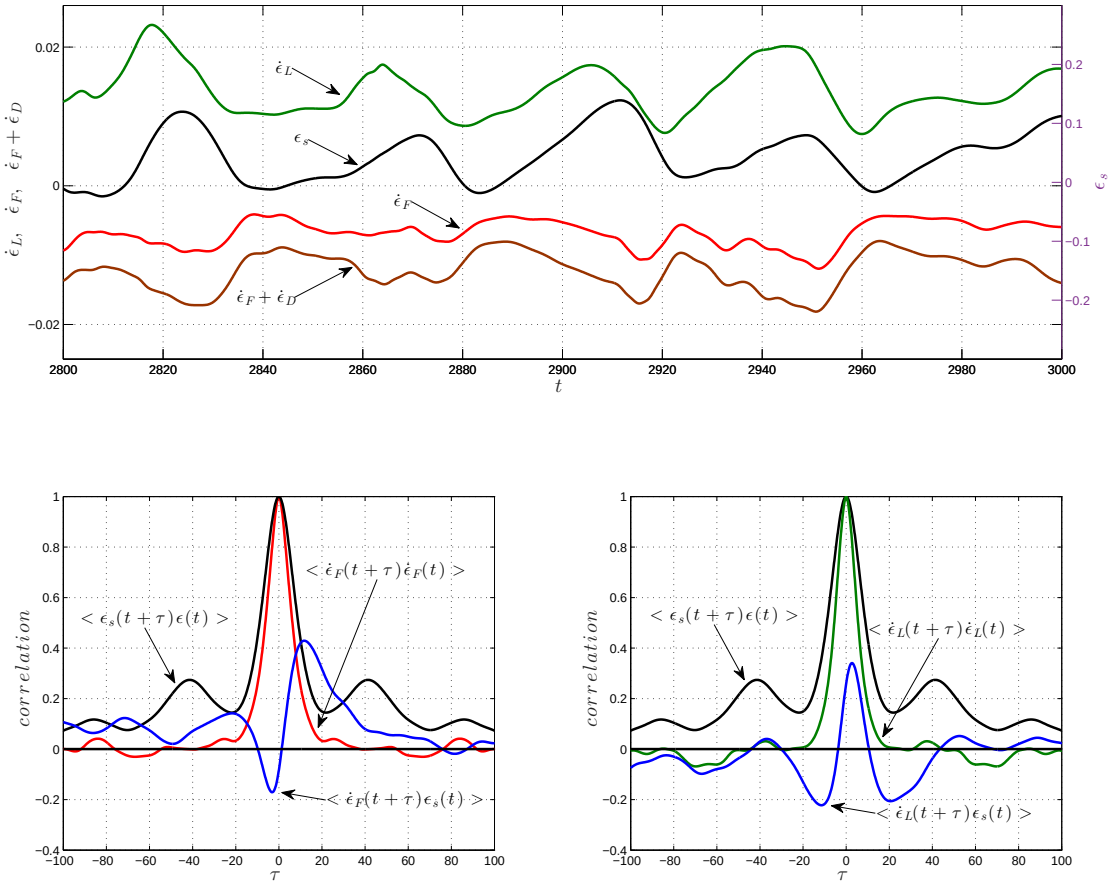

FIG. 21: Time series of the time rate of the rms streak amplitude $\sqrt{\epsilon_s}$ in an RNL simulation (curve 1). Indicated contributions are mean advection (curve 2 with primary contribution from the lift up term $-\int U_s V \partial_y U dydz$), perturbation Reynolds stress (curve 3 with primary contribution from the spanwise component of the Reynolds stress divergence $-\int U_s \partial_z \overline{(uw)} dydz$) and from the dissipation (curve 4).

J. **727**, 127 (2011).

[20] K. Srinivasan and W. R. Young, J. Atmos. Sci. **69**, 1633 (2012).

[21] J. Jiménez, Phys. Fluids **25**, 101302 (2013).

[22] Parametric instability usually refers to the instability of a periodically modulated system (cf. [38], section 48). We use this term to refer to any linear instability that is inherently caused by the time dependence of the system. The reason we have adopted the same word to describe the instability of periodic and non-periodic flows is that the same instability mechanism operates in both cases as discussed by [33, 34].

[23] N. C. Constantinou, A. Lozano-Durán, M.-A. Nikolaidis, B. F. Farrell, P. J. Ioannou, and J. Jiménez, J. Phys. Conf. Ser. **506**, 012004 (2014).

[24] V. Thomas, B. K. Lieu, M. R. Jovanović, B. F. Farrell, P. J. Ioannou, and D. F. Gayme, Phys. Fluids **26**, 105112 (2014).

[25] V. Thomas, B. F. Farrell, P. J. Ioannou, and D. F. Gayme, Phys. Fluids **27**, 105104 (2015).

[26] J. U. Bretheim, C. Meneveau, and D. F. Gayme, Phys. Fluids **27**, 011702 (2015).

[27] B. F. Farrell, P. J. Ioannou, J. Jiménez, N. C. Constantinou, A. Lozano-Durán, and M.-A. Nikolaidis, J. Fluid Mech. (2015), (submitted, arXiv:1512.06018 [physics.flu-dyn]).

[28] M.-A. Nikolaidis, B. F. Farrell, P. J. Ioannou, D. F. Gayme, A. Lozano-Durán, and J. Jiménez, J. Phys.: Conf. Ser. **708**, 012002 (2016).

[29] C. Foias, O. Manley, R. Rosa, and R. Temam, *Navier-Stokes Equations and Turbulence* (Cambridge University Press, Cambridge, 2001).

[30] E. Hopf, J. Ration. Mech. Anal. **1**, 87 (1952).

[31] U. Frisch, *Turbulence: The Legacy of A. N. Kolmogorov* (Cambridge University Press, 1995).

[32] J. B. Marston, Annu. Rev. Condens. Matter Phys. **3**, 285 (2012).

[33] B. F. Farrell and P. J. Ioannou, J. Atmos. Sci. **53**, 2041

(1996).
[34] B. F. Farrell and P. J. Ioannou, J. Atmos. Sci. **56**, 3622 (1999).
[35] B. F. Farrell and P. J. Ioannou, Stochastic Dyn. **2**, 395 (2002).
[36] B. F. Farrell and P. J. Ioannou, J. Atmos. Sci. **59**, 2647 (2002).
[37] N. C. Constantinou, B. F. Farrell, and P. J. Ioannou, J. Atmos. Sci. **71**, 1818 (2014).
[38] P. G. Drazin and W. H. Reid, *Hydrodynamic Stability* (Cambridge University Press, Cambridge, 1981).